ORIGINAL ARTICLE

ACTA RADIOLOGICA

Transcatheter Coil Embolization for Steal Syndrome in Patients with Hemodialysis Access

S. KARIYA[1], N. TANIGAWA[1], H. KOJIMA[1], A. KOMEMUSHI[1], Y. SHOMURA[1], T. SHIRAISHI[2], T. KAWANAKA[3] & S. SAWADA[1]

[1]Department of Radiology, Kansai Medical University, Osaka, Japan, [2]Department of Radiology and [3]Department of Urology, Ishikiri Seiki Hospital, Osaka, Japan

Kariya S, Tanigawa N, Kojima H, Komemushi A, Shomura Y, Shiraishi T, Kawanaka T, Sawada S. Transcatheter coil embolization for steal syndrome in patients with hemodialysis access. Acta Radiol 2009;50:28–33.

Background: Drainage of large amounts of shunt blood into deep veins via collaterals reduces resistance to venous outflow and decreases blood flow to the artery distal to the arterial anastomotic site, potentially resulting in steal syndrome.

Purpose: To evaluate the effectiveness of transcatheter coil embolization for collateral veins of hemodialysis access in the treatment of steal syndrome.

Materials and Methods: Five hemodialysis patients (four male, one female; mean age 58.8 years, range 40–71 years) with symptomatic steal syndrome were treated. Steal syndrome was diagnosed based on decreased or absent distal pulse, coolness, pain, abnormal skin color, ischemic ulceration of digits, numbness, sensory impairment, or motor impairment. Coil embolization was performed to block collaterals communicating with deep veins, with conscious sedation and local anesthesia. Fistulography was performed before, immediately after, and 1 month after embolization. Ultrasonography was performed 2 days after embolization. Symptoms and signs were assessed 2 days after embolization. Clinical findings related to steal syndrome and access failure were observed at each hemodialysis.

Results: Blood flow in the collaterals was successfully blocked by coil embolization in all patients. Distal pulse, coolness, pain, and skin color improved in all patients. Numbness, sensory impairment, and motor impairment were unimproved in two patients. In all patients, hemodialysis following embolization was performed normally. The mean observation period after embolization was 33 months (range 9–75 months).

Conclusion: Coil embolization of collaterals that drain shunt blood into deep veins is effective for steal syndrome for hemodialysis access originating in the brachial artery.

Key words: Adults; embolization; interventional; ischemia; vascular; vein

Shuji Kariya, Department of Radiology, Kansai Medical University, 2-3-1 Shinmachi, Hirakata, Osaka, 573-1192, Japan (tel. +81 72 804 0101, fax. +81 72 804 2865, e-mail. shauji@ops.dti.ne.jp)

Accepted for publication September 30, 2008

About 1% of patients with distal forearm arteriovenous (AV) fistulas and about 3–6% of patients with AV fistulas or AV grafts originating in the brachial artery display severe ischemic symptoms requiring treatment (1–5). Several surgical treatments have been devised for treatment of distal ischemia, such as access ligation, banding, and distal revascularization-interval ligation (6–8). Access ligation and banding are widely used. The banding technique is based on the concept that increasing resistance to fistula outflow will result in increased flow in the portion of the artery distal to the fistula (6, 7). The problem with this procedure is the difficulty in determining the required amount of stenosis.

Drainage of large amounts of shunt blood into deep veins via collaterals reduces resistance to fistula outflow and decreases blood flow to the artery distal to the arterial anastomotic site. Our therapeutic technique for steal syndrome is to block collaterals draining into deep veins that are unsuitable as hemodialysis access using coil embolization, and the basic concept behind this technique is to increase resistance to fistula outflow, as in surgical banding (6, 7).

informa
healthcare

DOI 10.1080/02841850802537933

The purpose of our study was to evaluate the effectiveness of transcatheter coil embolization for collateral veins of hemodialysis access in the treatment of steal syndrome.

Material and Methods

All study protocols were approved by our institutional review board, and written informed consent was obtained from all patients prior to participation. The present study was conducted from November 2001 to February 2008 in our institution, which has the capacity to provide hemodialysis to 400 chronic renal failure patients.

Patients and inclusion criteria

Five patients (four male, one female; mean age 58.8 years, range 40–71 years) were treated. Their characteristics, symptoms, and signs are shown in Table 1. Patients with chronic renal failure who satisfied the following inclusion criteria were enrolled in the study: 1) presence of AV fistulas or AV grafts originating in the brachial artery for hemodialysis; 2) diagnosis of steal syndrome; 3) access displaying collaterals shunting blood into deep veins that could not be used for hemodialysis access; and 4) manual compression of collaterals restores distal pulses by palpation.

Steal syndrome was diagnosed based on symptoms and signs, as defined by decreased or absent distal pulse, coolness, pain, abnormal skin color, ischemic ulceration of digits, numbness, sensory impairment, or motor impairment. Bedside palpation and auscultation were performed to confirm the existence of an outflow vein to be used as hemodialysis access (main outflow vein) and collaterals that drained into deep veins that were unsuitable for hemodialysis access. Collateral outflow veins were manually compressed, and restoration of distal pulses was confirmed by palpation.

In all patients, before the current hemodialysis access was created, hemodialysis was performed using an AV fistula created on the ipsilateral forearm. When this hemodialysis access failed, the current AV fistula or graft originating in the brachial artery was created.

Procedures

All procedures were performed on an outpatient basis with conscious sedation (midazolam; Yamanouchi Pharmaceutical, Tokyo, Japan).

In all patients, a 5F introducer sheath (Medikit, Miyazaki, Japan) was placed in the outflow vein or

Table 1. Patients and symptoms

Patient	1	2	3	4	5
Age, years	40	50	71	65	69
Sex	M	M	F	M	M
Diabetes	+	+	–	–	–
Type of access	AVF	AVF	AVG	AVF	AVF
Kind of anastomosis	Brachiocephalic AVF	Brachiocephalic AVF	Brachiobasilic AVG	Brachiocephalic AVF	Brachiobasilic AVF
Localization of anastomosis	Elbow	Elbow	Elbow	Elbow	Elbow
Current access age, days	34	65	123	1084	1283
Detection of brachial artery distal to the AV fistula in fistulography	–	–	*	–	–
Limb ischemia					
Decreased or absent distal pulses	+	+	+	+	+
Coolness	+	+	+	+	+
Pain during dialysis	+	+	+	+	+
Rest pain	+	+	+	+	+
Skin color	cyanosis	pallor	pallor	cyanosis	cyanosis
Ischemic ulcers	–	–	–	–	+
Gangrene	–	–	–	–	–
Neuropathy					
Numbness	+	+	–	–	–
Sensory impairment	+	+	–	–	–
Motor impairment	+	+	–	–	–

* Patient 3 underwent anterograde fistulography by injecting contrast medium from the graft.
AVF: arteriovenous fistula; AVG: arteriovenous graft.

graft, with local anesthesia of 1% lidocaine hydrochloride (Xylocaine polyamp 1%; AstraZeneca, Osaka, Japan). Anterograde fistulography was obtained before coil embolization (Ultimax MSDX R0042EAD; Toshiba Medical Systems, Tochigi, Japan). At fistulography, contrast medium (370 mg I/ml Iopamiron; Nihon Schering, Osaka, Japan) was injected through a 21G elastor needle placed in the brachial artery or through a 5F introducer sheath in the graft. Fistulography findings were matched with the collateral outflow vein detected by bedside palpation and auscultation, and the collateral outflow vein was manually compressed again to confirm restoration of distal pulses by palpation. The collateral outflow vein was identified and catheterized selectively in all patients using a 5F catheter (Fansac; Clinical Supply, Gifu, Japan) or with a coaxially placed microcatheter (2.7F progreat [Terumo, Tokyo, Japan] or Tracke 18 [Boston Scientific, Natick, Mass., USA]) advanced through the 5F catheter. Additional coils were placed in the collateral outflow vein until shunt blood stopped draining into deep veins. If multiple collateral outflow veins displayed high levels of blood flow, as many veins as necessary were embolized. Collateral outflow veins with low blood flow were left untouched. Pushable fibered coils were used in four patients, while detachable coils were used in one patient.

Pushable fibered coils were 0.38" Fibered Platinum Embolization Coils (Boston Scientific, Natick, Mass., USA), 5–9 mm in unconstrained diameter; FPC35 VORTX -35 Vascular Occlusion Coils (Boston Scientific, Natick, Mass., USA), 5–6 mm in unconstrained diameter; TORNADO MWCE-35 embolization coils (Cook, Bloomington, Ind., USA), 8 mm in unconstrained diameter; or VORTX-18 Diamond Shape Coils (Boston Scientific, Natick, Mass., USA), 5–6 mm in unconstrained diameter. We used pushable coils with nominal diameters 10–40% larger than estimated diameter of the collateral outflow vein (i.e., oversizing).

In one patient, the diameter of the collateral outflow vein gradually increased downstream toward the deep veins from the location of coil placement. As coil migration was a possibility, DCS-18S-SPIRAL detachable coils (Cook, Bloomington, Ind., USA) of 6–14 mm in unconstrained diameter were used with a DLD-11/18-UNI detach locking device (Cook, Bloomington, Ind., USA).

In patient 1 alone, blood pressure in the anastomotic site was measured before and after coil embolization. After the procedure, blood pressure was measured to evaluate whether hemodialysis following coil embolization was normal or not. Symptoms and signs 2 days after coil embolization were also assessed. In all patients, ultrasonography was performed 2 days after coil embolization and fistulography was performed 1 month after coil embolization. Clinical findings related to steal syndrome and access failure were observed at each hemodialysis.

Complications were categorized as minor or major according to the published guidelines of the Society of Interventional Radiology (9).

Results

In all patients, blood flow in collateral outflow veins was successfully blocked by transcatheter coil embolization (Fig. 1). Table 2 shows the results after coil embolization. In patient 1, blood pressure at the anastomotic site was 61/39 mmHg before coil embolization and 101/54 mmHg after embolization.

In all patients, fistulography 1 month after coil embolization showed that blood flow in the coil-embolized collateral outflow veins was still blocked. In patients 1–4, no new collateral outflow veins were seen, while patient 5 showed some new collaterals that were thin and superficial. In patient 3, fistulography showed that, 1 month after coil embolization, the main outflow vein was enlarged compared to before coil embolization. In patient 1, fistulography was performed 33 months after coil embolization, as the venous pressure in the main outflow vein increased. On fistulography, the main outflow vein was enlarged and stenosis of the central region of the main outflow vein was confirmed. This stenosis was dilated by balloon angioplasty.

Patient 5 recovered from the ulcer without administration of prostaglandin 1 month after coil embolization. In patient 1, numbness and motor and sensory impairments gradually improved after coil embolization and resolved completely within 18 months. In patient 2, numbness and motor and sensory impairments had not improved 9 months after coil embolization. As a result, the AV fistula was surgically ligated 288 days after coil embolization, and superficialization of the brachial artery was performed on the contralateral upper arm. However, numbness and motor and sensory impairments were unimproved soon after ligation. The main outflow vein remained patent for 75 months in patient 1, 37 months in patient 3, 21 months in patient 4, and 24 months in patient 5. In all patients, ischemia of the limb distal to AV fistula or graft site did not recur.

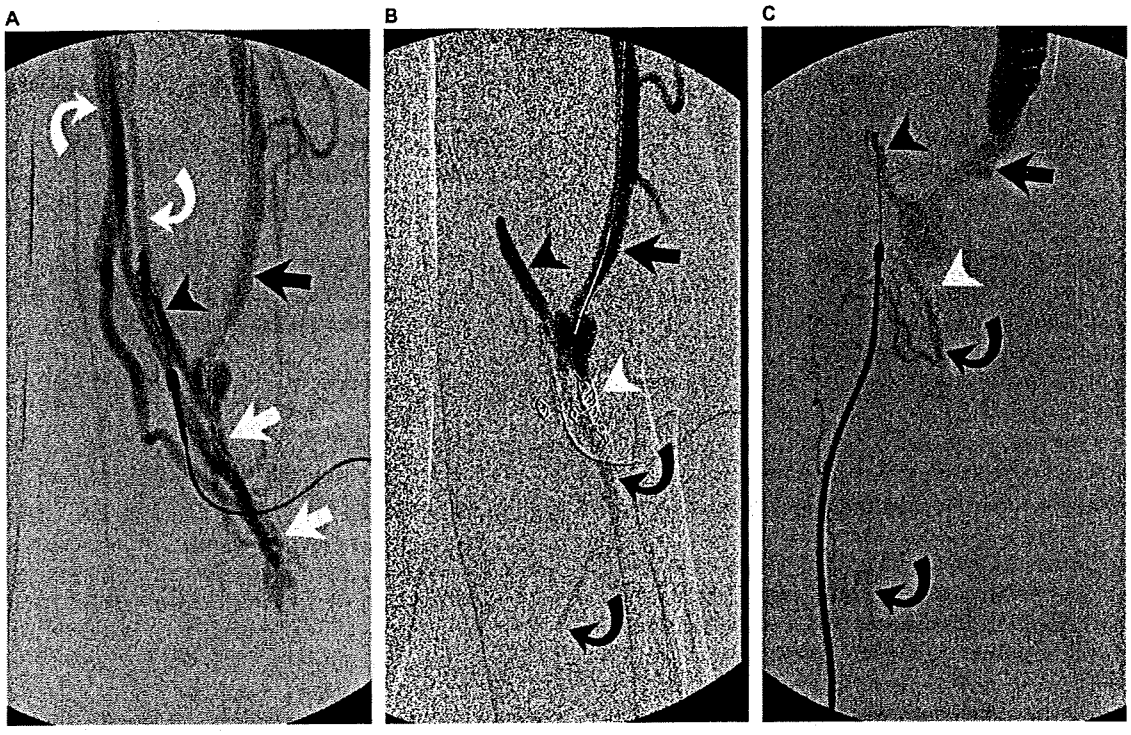

Fig. 1. Patient 1. Fistulography in a 40-year-old man displaying steal syndrome with AV fistula originating in the brachial artery. All figures were obtained by anterograde fistulography, and contrast medium was injected through a 21G elastor needle placed in the brachial artery (black arrowheads). A. Fistulography before coil embolization. Beside the main outflow vein used as hemodialysis access (black arrow), collateral outflow veins (white arrows) drained shunt blood into deep veins (curved white arrows). The artery distal to the AV fistula site could not be depicted. B. Fistulography immediately after coil embolization. A coil (white arrowhead) was placed to embolize the collateral outflow vein. While drainage to deep veins was blocked, the main outflow vein (black arrow) was unaffected. Blood flow in the artery distal to the AV fistula site (curved black arrow) was weak but became anterograde. C. Fistulography following balloon angioplasty for main outflow vein stenosis at 33 months after coil embolization. Blood flow in the artery distal to the AV fistula site (curved black arrows) remained anterograde. The main outflow vein (black arrow) was dilated compared to at the time of coil embolization. The coil (white arrowhead) still blocked the collateral outflow vein.

In patients 3–5, minor complications of flare, pain, and heat sensation at the site of embolization were present starting on the day of coil embolization, and lasted for 3–8 days. Symptoms were limited to coil-embolized collateral outflow veins and improved without medication. No patients experienced coil migration during or after coil embolization, and no other complications were seen.

Discussion

As the patients in the present study had AV fistula on the ipsilateral forearm until the creation of the current hemodialysis access, collateral outflow and deep veins might have been dilated. In this state, shunt blood might be likely to drain into deep veins via collateral outflow veins bifurcating from main outflow veins near the anastomotic site, potentially reducing resistance to fistula outflow and decreasing blood flow in the artery distal to the arterial anastomotic site.

In our patients with shunt blood draining into deep veins, peripheral circulatory failure due to venous hypertension might represent one cause of hand ischemia. Although no typical clinical findings of venous hypertension were noted in our patients, it was not possible to clarify this in the study.

Symptoms attributable to ischemia improved in all patients, so transcatheter coil embolization of collateral outflow veins appears to offer a feasible method of treatment for steal syndrome. The basic concept of our technique is to increase resistance to fistula outflow, as seen with surgical banding (6, 7). In patient 1, blood pressure at the anastomotic site increased immediately after coil embolization, suggesting increased resistance to fistula outflow.

The presence of a collateral outflow vein draining a large amount of shunt blood to deep veins was confirmed by bedside palpation and auscultation,

Table 2. Results after coil embolization

Patient	1	2	3	4	5
Number of coils used					
Pushable coils	5	5	7	0	20
Detachable coils	0	0	0	8	0
Detection of brachial artery distal to AV fistula in fistulography	+	+	*	+	–
Hemodialysis after coil embolization	normal	normal	normal	normal	normal
Limb ischemia					
Decreased or absent distal pulses	–	–	–	–	+
Coolness	–	–	–	–	–
Pain during dialysis	–	–	–	–	–
Rest pain	–	–	–	–	–
Skin color	normal	normal	normal	normal	normal
Ischemic ulcers	–	–	–	–	–
Gangrene	–	–	–	–	–
Neuropathy					
Numbness	+	+	–	–	–
Sensory impairment	+	+	–	–	–
Motor impairment	+	+	–	–	–

* Patient 3 underwent anterograde fistulography, by injecting contrast medium from the graft.
AV: arteriovenous.

and we determined whether to perform coil embolization by manually compressing the collateral outflow vein. Selection of patients meeting the indications for our method of treatment before fistulography thus appears feasible.

The reason for using detachable coils in one patient was that coil migration was possible based on location and blood flow. In this patient, coils were placed over the bifurcation for multiple collateral outflow veins. When the diameter of collateral outflow veins gradually increases downstream toward the deep veins, the risk of coil migration requires attention.

In two patients, numbness and motor and sensory impairments did not improve immediately after coil embolization. These cases appear to have involved ischemic monomelic neuropathies that were irreversible (10–13).

Enlargement of the main outflow vein was confirmed in two patients (40%). As a result, our technique may have excessively developed the main outflow vein. One patient displayed increased venous pressure 33 months after coil embolization due to stenosis of the central region of the main outflow vein. This might have been attributable to blockage of collaterals draining shunt blood into deep veins, thus increasing blood flow in the main outflow vein.

Fever, pain, and flare in three patients after coil embolization were typical symptoms of thrombophlebitis. Thrombotic occlusion was not seen in veins by ultrasonography, excluding embolized veins. We will thus be able to use the brachial or basilic vein as a drainage vein when new surgical reconstruction of hemodialysis access becomes necessary.

One advantage of our technique is that the same hemodialysis access used before therapy can be used without lowering blood flow in the main outflow vein. Conversely, banding lowers blood flow in the main outflow vein. Adjustment of the blood flow by banding is difficult and may cause thrombosis of hemodialysis access (14, 15).

We did not evaluate quantitatively the results before and after embolization. However, quantitative evaluation of blood flow and digital pressure may be done for an objective evaluation of the treatment results (16, 17). Our technique is unsuitable for steal syndrome in which excessive shunt blood is drained into the collateral outflow vein for access, because access could be lost following embolization.

In conclusion, coil embolization of collaterals that drain shunt blood into deep veins that cannot be used for hemodialysis access is effective for steal syndrome associated with AV fistula or graft originating in the brachial artery.

Declaration of interest: The authors report no conflicts of interest. The authors alone are responsible for the content and writing of the paper.

References

1. Duncan H, Ferguson L, Faris I. Incidence of the radial steal syndrome in patients with Brescia fistula for hemodialysis: its clinical significance. J Vasc Surg 1986; 4:144–7.
2. Haimov M, Burrows L, Schanzer H, Neff M, Baez A, Kwun K, et al. Experience with arterial substitutes in the construction of vascular access for hemodialysis. J Cardiovasc Surg (Torino) 1980;21:149–54.
3. Porter JA, Sharp WV, Walsh EJ. Complications of vascular access in a dialysis population. Curr Surg 1985; 42:298–300.
4. Zibari GB, Rohr MS, Landreneau MD, Bridges RM, DeVault GA, Petty FH, et al. Complications from permanent hemodialysis vascular access. Surgery 1988; 104:681–6.
5. Winsett OE, Wolma FJ. Complications of vascular access for hemodialysis. South Med J 1985;78:513–7.
6. Corry RJ, Patel NP, West JC. Surgical management of complications of vascular access for hemodialysis. Surg Gynecol Obstet 1980;151:49–54.
7. Morsy AH, Kulbaski M, Chen C, Isiklar H, Lumsden AB. Incidence and characteristics of patients with hand ischemia after a hemodialysis access procedure. J Surg Res 1998;74:8–10.
8. Berman SS Gentile AT Glickman MH Mills JL Hurwitz RL Westerband A et al. Distal revascularization-interval ligation for limb salvage and maintenance of dialysis access in ischemic steal syndrome. J Vasc Surg 1997;26:393–402; discussion 402.
9. Aruny JE, Lewis CA, Cardella JF, Cole PE, Davis A, Drooz AT, et al. Quality improvement guidelines for percutaneous management of the thrombosed or dysfunctional dialysis access. Standards of Practice Committee of the Society of Cardiovascular & Interventional Radiology. J Vasc Interv Radiol 1999;10: 491–8.
10. Bolton CF, Driedger AA, Lindsay RM. Ischaemic neuropathy in uraemic patients caused by bovine arteriovenous shunt. J Neurol Neurosurg Psychiatry 1979;42:810–4.
11. Wilbourn AJ, Furlan AJ, Hulley W, Ruschhaupt W. Ischemic monomelic neuropathy. Neurology 1983;33: 447–51.
12. Hye RJ, Wolf YG. Ischemic monomelic neuropathy: an under-recognized complication of hemodialysis access. Ann Vasc Surg 1994;8:578–82.
13. Redfern AB, Zimmerman NB. Neurologic and ischemic complications of upper extremity vascular access for dialysis. J Hand Surg [Am] 1995;20:199–204.
14. Ebeid A, Saranchak HJ. Banding of a PTFE hemodialysis fistula in the treatment of steal syndrome. Clin Exp Dial Apheresis 1981;5:251–7.
15. Dally P, Brantigan CO. Plethysmography and the diagnosis of the steal syndrome following placement of arteriovenous fistulas and shunts for hemodialysis access. J Cardiovasc Surg (Torino) 1987;28:200–3.
16. Wixon CL, Hughes JD, Mills JL. Understanding strategies for the treatment of ischemic steal syndrome after hemodialysis access. J Am Coll Surg 2000;191: 301–10.
17. Schanzer H, Eisenberg D. Management of steal syndrome resulting from dialysis access. Semin Vasc Surg 2004;17:45–9.

Cardiovasc Intervent Radiol (2008) 31:86–90
DOI 10.1007/s00270-007-9189-0

CLINICAL INVESTIGATION

Hepatic Arterial Infusion Chemotherapy through a Port-Catheter System as Preoperative Initial Therapy in Patients with Advanced Liver Dysfunction due to Synchronous and Unresectable Liver Metastases from Colorectal Cancer

Toshihiro Iguchi · Yasuaki Arai · Yoshitaka Inaba · Hidekazu Yamaura · Yozo Sato · Masaya Miyazaki · Hiroshi Shimamoto

Received: 5 June 2007 / Accepted: 11 September 2007 / Published online: 10 October 2007

Abstract
Purpose We retrospectively evaluated the safety and efficacy of preoperative initial hepatic arterial infusion chemotherapy (HAIC) through a port-catheter system in patients with liver dysfunction due to synchronous and unresectable liver metastases. The aim of HAIC was to improve patients' clinical condition for later surgical removal of primary colorectal cancer.
Methods Port-catheter systems were placed radiologically in 21 patients (mean age 58.6 ± 8.1 years) with liver dysfunction due to synchronous liver metastases from colorectal cancer. Initial HAIC of 1,000 mg/m^2 5-fluorouracil was administered weekly as a 5 hr continuous infusion through this system. Surgical removal of the primary lesion was planned after HAIC improved the liver function.
Results Port-catheter system placement was successful in all patients without severe complications. Patients were followed up for a median of 309 days (range 51–998 days). After starting HAIC, no severe adverse events that caused drug loss and treatment postponement or suspension were observed in any of the patients. HAIC was performed a mean of 4.5 ± 3.0 times and the liver function improved in all patients. Curative (n = 18) or palliative (n = 1) surgical removal of the primary lesion was performed. The remaining 2 patients died because extrahepatic metastases developed and their performance status worsened; thus, surgery could not be performed. The median survival times of all patients and the operated patients were 309 and 386 days, respectively.
Conclusion Initial HAIC administration is a safe and efficacious method for improving liver function prior to operative resection of primary colorectal cancer in patients with liver dysfunction due to synchronous and unresectable liver metastases.

Keywords Colorectal cancer · Hepatic arterial infusion chemotherapy · Liver metastasis · Port-catheter system

Introduction

Colorectal cancer is the fourth most commonly diagnosed malignant disease worldwide [1], and synchronous liver metastases are identified in 10–20% of cases [2]. However, the treatment protocol for patients with stage IV colorectal cancer with synchronous liver metastases has not been firmly established [2, 3]. In such patients, the choice of treatment strategy differs based on various factors such as liver function, the patient's condition, the urgency of operating on the primary lesion, and the institution's protocols for dealing with liver metastases and primary lesions. For the primary lesion, it is desirable that surgical removal is selected to improve the quality of life of the patients, because colorectal cancer may cause obstruction, perforation, bleeding, or pain [3]. Additionally it has been reported that stage IV patients who underwent resection of their asymptomatic primary lesions had prolonged median and 2-year survival periods compared with stage IV

T. Iguchi · Y. Inaba (✉) · H. Yamaura · Y. Sato · M. Miyazaki · H. Shimamoto
Department of Diagnostic and Interventional Radiology, Aichi Cancer Center Hospital, 1-1 Kanokoden, Nagoya, Chikusa-ku 464-8681, Japan
e-mail: 105824@aichi-cc.jp

Y. Arai
Department of Diagnostic Radiology, National Cancer Center Hospital, 5–1–1, Tsukiji, Tokyo, Chuo-ku 104–0045, Japan

was inserted from the left subclavian artery and advanced to the common hepatic artery via the celiac artery. Then an indwelling catheter (Anthron P-U catheter; Toray Medical, Tokyo, Japan or W spiral catheter; PIOLAX, Yokohama, Japan) with a side hole was inserted using the catheter-exchange method. The catheter tip was inserted into the deep segment of the gastroduodenal artery so that the side hole was placed into the common hepatic artery. The gastroduodenal artery around the tip of the indwelling catheter was embolized using microcoils and a mixture (1:1.5) of *n*-butyl cyanoacrylate (NBCA; Histoacryl; Braun, Melsungen, Germany) and iodized oil (Lipiodol Ultrafluide; Laboratoire Guerbet, Roissy, France) through a microcatheter inserted coaxially via the 5 Fr angiographic catheter inserted from the right femoral artery. Finally, the proximal end of the indwelling catheter was connected to a port implanted in the subcutaneous pocket created in the left chest wall.

Digital subtraction angiography and CT were performed during injection of contrast medium through the implanted port-catheter system within a few days of implantation to confirm that the catheter was not dislodged and that the entire liver was perfused adequately. Thereafter, HAIC was administered through this system: 1,000 mg/m^2 of 5-fluorouracil (5-FU) weekly by continuous 5 hr infusion [7]. After administration of the chemotherapeutic agent, the implanted port-catheter system was flushed and filled with 2 ml of heparin solution (1,000 IU/ml).

Statistical Analysis

The success rate and the complications of the placement of the port-catheter system were evaluated. After starting HAIC the clinical course, including improvement in liver function tests, performance of surgery, and survival were evaluated. In patients who underwent surgical removal of the primary lesion, the frequency of HAIC administration, time between the placement of the port-catheter system and surgery, details of the surgery, postoperative therapy, and survival were evaluated. The Wilcoxon signed rank test was used to compare the liver functions before surgery with those before starting HAIC. The cumulative survival rate was calculated using the Kaplan-Meier method.

A p value of less than .05 was considered significant.

Results

After placement of the port-catheter system, patients were followed up for a median of 309 days (range 51–998 days).

Placement of the Port-Catheter System

The radiological placement of the port-catheter system was successful in all 21 patients. During and after the procedure, there were no complications such as hematoma, subclavian or vertebral artery thrombosis, infections, hepatic artery occlusions, and catheter malfunctions.

Clinical Course after Starting HAIC

After starting HAIC, no severe adverse events that caused drug loss and treatment postponement or suspension were observed in any of the patients. HAIC was performed a mean of 4.5 ± 3.0 times (range 1–15 times) and the liver function improved in all 21 patients. In particular, the AST, ALT, LDH, ALP, and GTP levels were improved significantly (Table 1). In 19 of 21 patients, curative (n = 18) or palliative (n = 1) surgical removal of the primary lesion was performed. In the remaining 2 patients, although the liver function had improved after HAIC was administered 15 times and 5 times, respectively, extrahepatic metastases in the lung, bone or peritoneum developed rapidly and their performance status worsened. Though systemic chemotherapy was administered with or instead of HAIC afterward, they died 186 and 51 days, respectively, after the placement of port-catheter system; thus, surgery could not be performed.

Among the 19 patients who underwent surgery, HAIC was administered a mean of 3.9 ± 1.8 times (range 1–9 times), and the median period between placement of the

Table 1 Liver function before and after HAIC administration

		Before starting HAIC	After HAIC	p value
AST (IU/l)	Mean	110 ± 109	56 ± 55	
	Range	21–549	21–273	0.0001*
ALT (IU/l)	Mean	59 ± 43	31 ± 22	
	Range	17–183	11–101	0.0005*
T-BIL (mg/dl)	Mean	1.0 ± 0.5	1.2 ± 1.1	
	Range	0.3–2.2	0.3–4.4	0.717
LDH (IU/l)	Mean	1242 ± 1002	551 ± 501	
	Range	221–3870	174–2050	<0.0001*
ALP (IU/l)	Mean	874 ± 570	663 ± 526	
	Range	416–2660	124–2335	0.0046*
GTP (IU/l)	Mean	393 ± 433	207 ± 169	
	Range	130–2023	9–602	0.0061*

AST, aspartate aminotransferase; ALT, alanine aminotransferase; T-BIL, total bilirubin; LDH, lactate dehydrogenase; ALP, alkaline phosphatase; GTP, gamma-glutamyl transpeptidase; HAIC, hepatic arterial infusion chemotherapy

*Significant at $p < 0.05$

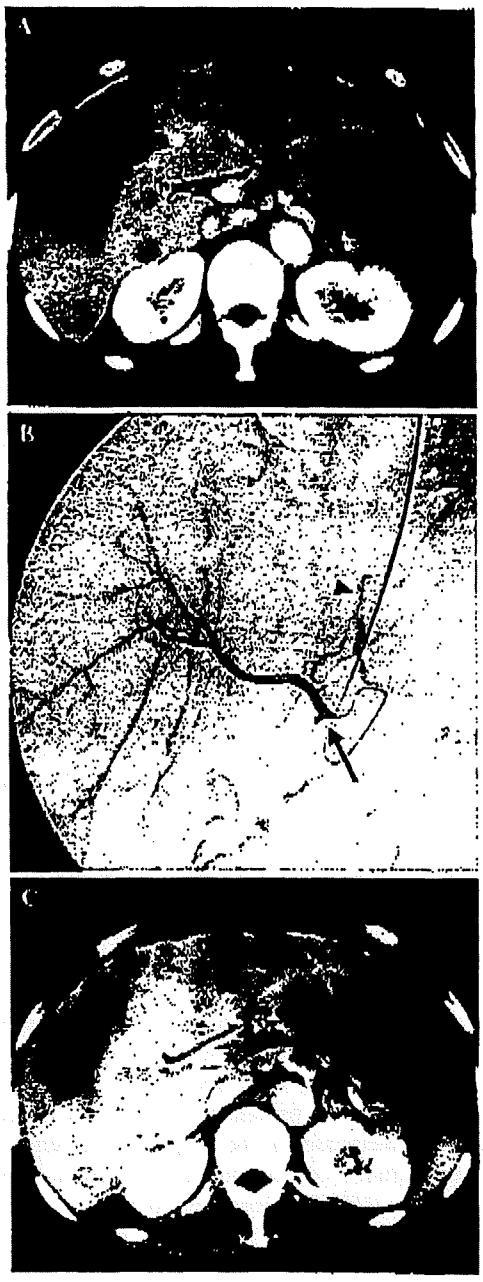

Fig. 2 A–C. A 55-year-old man with multiple liver metastases from rectal cancer. A Contrast-enhanced CT scan obtained before starting HAIC shows unresectable multiple liver metastases in both the right and left lobes. B An arteriogram via the port obtained before starting HAIC shows that all hepatic arteries are well visualized. The catheter tip was inserted into the deep segment of the gastroduodenal artery and embolized using microcoils and a mixture of *n*-butyl cyanoacrylate and iodized oil. The side hole was placed into the common hepatic artery (arrow). The accessory left hepatic artery, which branched from the left gastric artery, was embolized with microcoils (arrowhead) in order to establish hepatic arterial supply from a single vessel. C Contrast-enhanced CT scan obtained after five HAIC administrations shows slightly smaller multiple liver metastases. With the exception of T-BIL, the patient's liver function improved (AST improved from 83 to 26 IU/l, ALT improved from 49 to 18 IU/l, LDH improved from 1,155 to 458 IU/l, and ALP improved from 950 to 502 IU/l)

port-catheter system and surgery was 29 days (range 14–68 days). Of 13 patients who had no extrahepatic metastases prior to the surgery, 10 developed extrahepatic metastases. Among 16 of 19 patients, systemic chemotherapy with or instead of HAIC was administered after the surgery.

The overall median survival time of all the patients was 309 days and that of the patients who underwent surgery was 386 days (Fig. 1). At present, 20 patients have died.

A representative case is shown in Fig. 2.

Discussion

Many studies have reported the effectiveness of HAIC administration through a port-catheter system for liver metastases from colorectal cancer [6–8]. In Western countries, it has been reported that HAIC is effective in treating liver metastases; however, it does not improve the prognosis [6]. On the other hand, in Japan, good results have been reported after intermittent hepatic arterial infusion of a high dose of 5-FU: the response rate is reportedly 78% and the median survival time is 25.8 months [7].

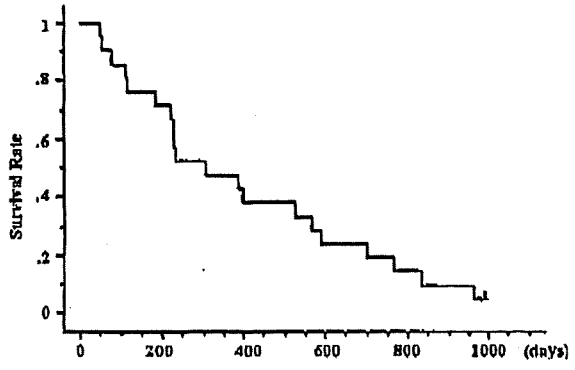

Fig. 1 Overall survival time

In general, systemic chemotherapy is usually selected for colorectal cancer with distant metastases [2]. Recently, the standard regimens such as FOLFILI (5-FU plus leucovorin with oxaliplatin) and FORFOX (5-FU plus leucovorin and irinotecan) are used, and the median survival after FOLFILI and FORFOX has been reported to be 12.6–21.5 months [12]. In many cases, systemic chemotherapy might be the first choice of treatment for patients with primary colorectal cancer and synchronous distant metastases, and we usually select systemic chemotherapy

as an initial therapy for such patients. Although it is doubtful whether the initial HAIC administration is effective in patients who have not undergone any therapy for the primary lesion, HAIC was administered initially in order to improve or control liver metastases. We judged that liver metastasis was the prognosis-limiting factor, because the liver dysfunction in these patients had already progressed due to liver metastases. Additionally, we aim to surgically remove the primary lesion later, if possible, because primary colorectal cancer may cause obstruction, perforation, bleeding, or pain [3]. Based on the results of this study, we believe that initial HAIC administration is effective because, in 19 of 21 patients, surgery was possible after the liver function had been improved by HAIC administration.

In the 19 patients who underwent surgery, HAIC administration was terminated 1 week before surgery to prevent its effect on surgery. The wide range of the frequency of HAIC administration was due to the fact that surgery was not performed until, in the surgeons' opinion, the patient's liver function had improved. We observed that the liver functions before surgery had improved significantly after HAIC administration compared with those before starting HAIC. It has been reported that HAIC has fewer side effects than systemic chemotherapy [13] and, in fact, we observed that surgeries could be performed without any adverse effects arising due to HAIC. We usually consider T-BIL >3.0 mg/dl or a performance status of 4 as the exclusion criteria for HAIC administration because, based on our experience, it is difficult to reduce such liver dysfunction and also improve performance status in patients. Further, the liver dysfunction of such patients may be adversely affected by HAIC administration. Based on our results, there were no severe adverse events after HAIC administration when these exclusion criteria were used for the selection of the candidates. In 2 of 21 patients, although the liver function improved after HAIC administration, surgery could not be performed because they developed extrahepatic metastases in the lung, bone or peritoneum, and their performance status worsened. Unfortunately, we cannot expect HAIC administration to have an anticancer effect on the entire body [7].

There were some limitations in our retrospective study. Firstly, the liver dysfunction of our patients was already advanced; therefore, we hesitated to administer systemic chemotherapy when malignancy was first identified. Secondly, in many patients, other distant metastases were present or developed and systemic chemotherapy was started after the surgery. We could not administer standard systemic chemotherapy such as FOLFILI and FORFOX, and our regimens of systemic chemotherapy were not established, because it is only recently that such standard regimens have been employed in practice in Japan. The survival period might have been prolonged if we had employed the currently used standard systemic chemotherapy.

In conclusion, initial HAIC administration is a safe and efficacious method for improving liver function prior to operative resection of primary colorectal cancer in patients with liver dysfunction due to synchronous and unresectable liver metastases.

References

1. Ferlay J, Bray F, Pisani P, Parkin DM (2004) GLOBOCAN 2002: Cancer incidence, mortality and prevalence worldwide. IARC CancerBase no. 5, version 2.0. IARC Press, Lyon, France
2. Alexander HR, Kemeny NE, Lawrence TS (2000) Metastatic cancer to the liver. In: DeVita VT (ed) Cancer, 7th edn. Williams & Wilkins, Baltimore, pp 2353–2368
3. Ruo L, Gougoutas C, Paty PB, et al. (2003) Elective bowel resection for incurable stage IV colorectal cancer: Prognostic variables for asymptomatic patients. J Am Coll Surg 196:722–728
4. Tanaka T, Arai Y, Inaba Y, et al. (2003) Radiologic placement of side-hole catheter with tip fixation for hepatic arterial infusion chemotherapy. J Vasc Interv Radiol 14:63–68
5. Yamagami T, Iida S, Kato T, et al. (2002) Using *n*-butyl cyanoacrylate and the fixed-catheter-tip technique in percutaneous implantation of a port-catheter system in patients undergoing repeated hepatic arterial chemotherapy. AJR Am J Roentgenol 179:1611–1617
6. Meta-Analysis Group in Cancer (1996) Reappraisal of hepatic arterial infusion in the treatment of nonresectable liver metastases from colorectal cancer. J Natl Cancer Inst 88:252–258
7. Arai Y, Inaba Y, Takeuchi Y, et al. (1997) Intermittent hepatic arterial infusion of high-dose 5FU on a weekly schedule for liver metastases from colorectal cancer. Cancer Chemother Pharmacol 40:526–530
8. Link KH, Sunclaitis E, Kornmann M, et al. (2001) Regional chemotherapy of nonresectable colorectal liver metastases with mitoxantrone, 5-fluorouracil, folinic acid, and mitomycin C may prolong survival. Cancer 92:2746–2753
9. Oken MM, Creech RH, Tormey DC, et al. (1982) Toxicity and response criteria of the Eastern Cooperative Oncology Group. Am J Clin Oncol 5:649–655
10. Arai Y, Inaba Y, Takeuchi Y (1997) Interventional techniques for hepatic arterial infusion chemotherapy. In: Castaneda-Zuniga WR (ed) Interventional radiology, 3rd edn. Williams & Wilkins, Baltimore, pp 192–205
11. Inaba Y, Arai Y, Matsueda K, et al. (2001) Right gastric artery embolization to prevent acute gastric mucosal lesions in patients undergoing repeat hepatic arterial infusion chemotherapy. J Vasc Interv Radiol 12:957–963
12. Kelly H, Goldberg RM (2005) Systemic therapy for metastatic colorectal cancer: Current options, current evidence. J Clin Oncol 23:4553–4560
13. Collins JM (1984) Pharmacokinetic rationale for intra-arterial therapy. In: Howell SB (ed) Intra-arterial and intracavitary cancer chemotherapy. Martinus Nijhoff, Boston, pp 1–10

Original Research

Equivalent Cross-Relaxation Rate Imaging of Axillary Lymph Nodes in Breast Cancer

Shigeru Mastsushima, RT, PhD,[1*] Hideyuki Nishiofuku, MD,[2] Hiroji Iwata, MD, PhD,[3] Seiichi Era, MD, PhD,[4] Yoshitaka Inaba, MD, PhD,[5] and Yasutomi Kinosada, MD, PhD[1]

Purpose: To determine whether equivalent cross-relaxation rate (ECR) imaging (ECRI) is a feasible method for optimization of axillary lymph node dissection (ALND) and thereby improve quality-of-life (QOL).

Materials and Methods: A total of 50 breast cancer patients underwent ECRI, with off-resonance saturation pulse at frequency offset of 5 ppm. ECR threshold values were determined to evaluate metastases to lymph nodes in the ALND group before examining the relationship between ECR value and cellular density. Metastases to lymph nodes of the sentinel lymph node biopsy (SLNB) group were evaluated based on the results of the ALND group.

Results: In the ALND group, regions without metastases showed a higher cellular density and ECR value than those with metastases. The relationship of ECR value to cellular density formed two clusters according to the presence or absence of metastasis; cellular density was related to ECR value for both clusters. In the SLNB group, supposing a threshold ECR value of 80%, sensitivity and specificity were 88.2% and 100%, respectively.

Conclusion: ECRI is a potentially useful method for cellular density imaging of axillary lymph nodes. ECRI provides active information that enables ALND to be avoided, thus improving QOL.

Key Words: sentinel lymph node; cellular imaging; molecular imaging; breast cancer; equivalent cross-relaxation rate; magnetization transfer
J. Magn. Reson. Imaging 2008;27:1278–1283.

LYMPHEDEMA IS A RELATIVELY COMMON, potentially serious, and unpleasant complication after axillary lymph node dissection (ALND) for breast cancer. It may be associated with functional, esthetic, and psychological problems, thereby affecting the quality-of-life (QOL) of breast cancer survivors. lymphedema also predisposes to the development of other secondary complications such as infections of the upper limb, psychological sequelae, development of malignant tumors, and deterioration in QOL (1). The risk of lymphedema is associated with the extent of ALND and the addition of axillary radiation therapy (1). Sentinel lymph node (SLN) biopsy (SLNB) is fast becoming the technique of choice for determining whether breast cancer has spread to lymph ducts or nodes. SNLB is only bypassed where significant evidence exists of clinical involvement of one or more axillary lymph nodes (2).

Molecular imaging is also instrumental in drug development, gene therapy, and in clinical research of breast cancer following the advent of fluorodeoxyglucose positron emission tomography and SLN techniques (3–5). While current methods are based on radio-lymphoscintigraphy (6), fluorescence lymphangiography (7) and magnetic resonance lymphangiography (MRL) (8) offer the benefits of improved spatial resolution without ionizing radiation. MRL is used for localizing SLNs in breast cancer; previous studies have reported the use of contrast agent (9–13).

In contrast, equivalent cross-relaxation rate (ECR) imaging (ECRI) is an MRI measurement method used to quantitatively evaluate a change in the protein–water interaction (14–18). Earlier studies further refined this technique and demonstrated that the cross-relaxation rate can be calculated using a simple equation; this was termed the ECR (14,15). In ECRI, the contrast obtained in breast cancer tissue has been shown to correlate with the malignant potential of cells and the extent of fibrosis (15,16).

It was reported that ECRI was related to changes in the macroscopic image and that it was possible to evaluate the presence or absence of axillary lymph node metastases using this technique (17,18). In the present study, we aimed to assess the precision of ECRI as a predictor of axillary lymph node metastasis to optimize ALND and improve QOL.

[1]Department of Biomedical Informatics, Gifu University Graduate School of Medicine, Gifu, Japan.
[2]Department of Radiology, Nara Medical University, Nara, Japan.
[3]Department of Breast Surgery, Aichi Cancer Center, Nagoya, Japan.
[4]Department of Physiology and Biophysics, Gifu University Graduate School of Medicine, Gifu, Japan.
[5]Department of Diagnostic and Interventional Radiology, Aichi Cancer Center, Nagoya, Japan.
Contract grant sponsor: JSPS, KAKENHI; Contract grant number: 19591409.
*Address reprint requests to: S.M., RT, PhD, Department of Biomedical Informatics, Gifu University Graduate School of Medicine, 1-1 Yanagido, Gifu 501-1194, Japan. E-mail: smts@gifu-u.ac.jp
Received July 30, 2007; Accepted February 7, 2008.
DOI 10.1002/jmri.21355
Published online in Wiley InterScience (www.interscience.wiley.com).

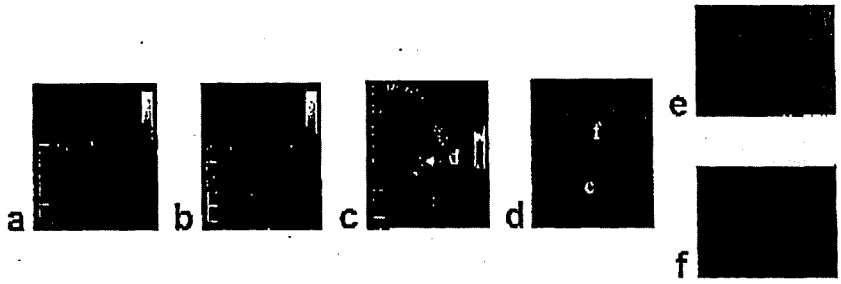

Figure 1. Axillary lymph node images of a patient with breast cancer. This lymph node shows inflammation without metastases. **a:** 3DSPGR image of an axillary lymph node. **b:** ST-3DSPGR image of an axillary lymph node. **c:** ECRI at frequency offset of 5 ppm. The lymph node shows high ECR (125.3% ± 15.2%) in the region that excludes adipose tissue, as shown in red on the ECRI. **d:** Macroscopic image of the lymph node (H&E stain; original magnification, ×5). **e:** High-power photomicrograph of normal lymph organization (H&E stain; original magnification, ×400). **f:** High-power photomicrograph of adipose tissue. (H&E stain; original magnification, ×400).

MATERIALS AND METHODS

Patient Population

The institutional ethics committee of our institution approved this study. There were 50 patients in this study, all with histologically-confirmed invasive ductal carcinoma (IDC) of the breast. These patients were divided into two groups: the ALND group and the SLNB group.

A total of 15 patients (mean age = 57 years; age range = 33–67 years) with axillary lymph nodes with the longest axis ≥20 mm (median size = 28 mm, range = 20–48 mm) were selected to receive total ALND (ALND group). In the ALND group, 40 lymph nodes (median size = 10 mm, range = 5–48 mm) were compared with the images selected and graded by the pathologist.

The remaining 35 patients (mean age = 59 years, range = 33–76 years), with histologically confirmed IDC of the breast and axillary lymph nodes with longest axis <20 mm (median size = 10 mm, range = 5–19 mm), were selected to receive SLNB (SLNB group).

Among the 35 patients in the SLNB group, 16 patients with a positive SLNB and two patients with a negative SLNB were selected to receive total ALND. The threshold ECR value was evaluated for 35 lymph nodes (median size = 10 mm, range = 5–19 mm) from the results of the ALND group. Patients' axillary lymph nodes were examined by MRI prior to SLNB or ALND.

MRI Technique

MR images were obtained using a Signa 1.5T clinical scanner equipped with a 5-inch surface coil. Two sets of coronal images were acquired in the plane of the axillary lymph nodes using two standard pulse sequences: three-dimensional spoiled gradient recalled acquisition in the steady state (3DSPGR) and saturation transfer prepared 3DSPGR (ST-3DSPGR). We adopted the off-resonance technique for preferential saturation of the immobile protons to evaluate the ECR values. The single magnetization transfer (MT) pulse frequency at an interval of 18 msec was employed at the frequency 5 ppm downfield from water resonance. The peak pulse amplitude was 3.26 μT for the MT sequence. This technique demonstrates a peak specific absorption rate of 2.89 W/kg, which is within the U.S. Food and Drug Administration (FDA) recommended value of 8 W/kg (19). MRI parameters were as follows: repetition time = 50 msec, echo time = 2.2 msec, flip angle = 30°, matrix size = 256 × 192, field of view = 20 cm, slice thickness = 5 mm, overlap locations = 0, and locations per slab = 16.

Postprocessing of MRI Data

The regions of interest (ROIs) for signal intensity measurements were selected from the axillary lymph nodes on the ipsilateral side. The ECR value was defined as

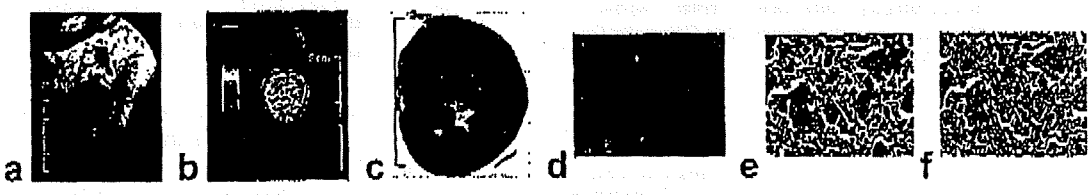

Figure 2. ECRI and photomicrograph of an axillary lymph node with metastases obtained from a patient with breast carcinoma. **a:** 3DSPGR image of the axillary lymph node. **b:** ECRI at frequency offset of 5 ppm. The region that does not contain metastases shows a high ECR value (114.4% ± 29.7%), as shown in red on the ECRI. In contrast, the region containing metastases shows a low ECR value (70.0% ± 12.0%), as shown in yellowish-green on the ECRI. **c:** Macroscopic image of the lymph node (H&E stain; original magnification, ×5). **d:** High-power photomicrograph demonstrating normal lymph organization (H&E stain; original magnification, ×400). **e:** High-power photomicrograph of the region that exhibited metastasis (H&E stain; original magnification, ×400). **f:** WinRoof image used in analyzing the cellular density in morphometry.

the percentage of signal loss between unsaturated and saturated images, as follows:

$$ECR\ (\%) = 100 \times (M_0/M_S - 1). \quad [1]$$

where M_0 and M_S are the signal intensity in the standard 3DSPGR and ST-3DSPGR images, respectively. The ECRIs were constructed based on the ECR value at each pixel and were calculated using Eq. [1].

Data Analysis

We first examined the correlation between the ECR values and the macroscopic histological images of the axillary lymph nodes in the ALND group; the ECR values of 40 lymph nodes were compared with the pathological images. The pathology specimens were stained with hematoxylin and eosin (H&E). In the measurement domain, the most typical location for metastasis, normal lymph organization, and adipose tissue were decided by a pathologist. Histopathological samples were obtained from the center of the axillary lymph nodes to confirm the relationship between the pathological findings and the ECRI. The ROI used for ECR had an ellipsoid sampling area of 6 mm^2. Between 5 and 110 ROIs were defined in each axillary lymph node; average ECR values were then calculated. We used the pathology specimens to help define ROIs for ECRI analysis.

We then evaluated the threshold ECR values of 35 lymph nodes from 35 patients in the SLNB group and compared these with the results from the ALND group. ROI for ECRI analysis was performed on these axillary lymph nodes. The ROI consisted of ellipsoids with a sampling area of 6 mm^2 for measurement of ECR. Between 5 and 50 ROIs were defined in each axillary lymph node. ECR measurement was performed in regions free of adipose tissue, as fat almost never displays a saturation transfer effect (17,18). The mean ECR value was assumed to be the ECR value of each lymph node.

WinRoof software was used to analyze the cellular density for morphometry. The ROIs had a rectangular sampling area of 340 μm^2 in the 400× microscope fields around which the apparently pathologic finding had been observed under lower magnification. Cell density was measured within 10 ROIs for each lymph node; the mean was assumed to be the cell density of each lymph node. In measurements of cellular density, the number of nuclei was obtained using a threshold setting for nuclear color extraction. In the present study, we assumed that the number of nuclei was similar to the number of cells.

The Mann-Whitney U test was employed to determine significant difference between the ECRs of regions containing metastases and those free of metastases. P values <0.05 were considered statistically significant.

RESULTS

Correlation of ECR and Pathological Diagnosis of Axillary Lymph Nodes in the ALND Group

Among the 40 lymph nodes, 15 had metastasis and 25 were free of metastasis. The average longest lymph node axes for metastatic and free nodes were 25.1 ± 11.2 mm and 9.1 ± 5.6 mm, respectively. There was a significant difference in lymph-node size between metastatic and free ($P < 0.001$); however, we did not observe a strong correlation between lymph-node size and ECR values (correlation coefficient = −0.41).

Figure 1 shows the axillary lymph node images of a patient with breast cancer. This lymph node shows inflammation without metastases, and the image reveals the location of adipose tissue in the central part of the lymph node. Figure 1a and b are 3DSPGR and ST-3DSPGR images; signal intensity is lower in Fig. 1b than in Fig. 1a. This reduction in signal intensity can be explained by the "saturation transfer effect." When this effect is large, the ECRI intensity (Fig. 1c) increases, as demonstrated by the ECRI calculated according to Eq. [1]. The ECR value of adipose tissue is close to 0%, shown as black and dark purple in Fig. 1c, and can be distinguished from other components because fat almost never displays a saturation transfer effect. Figure 1d is a pathology image that confirms that the ECR value of adipose tissue is close to 0%. Normal lymph node components show a high ECR (125.3% ± 15.2%) in regions without adipose tissue, as shown in red in Fig. 1c. Figure 1e and f are photomicrographs of normal lymph organization and adipose tissue, respectively. Normal lymph organization has a high cellular density, whereas that of adipose tissue is much lower.

The images in Fig. 2 show the axillary lymph nodes of a patient with breast cancer. The lymph node is metastatic, with most of the lymph node containing metastases. Figure 2a is a 3DSPGR image. As seen in Fig. 2b and c, the region without metastases displays a high ECR value (114.4% ± 29.7%), as shown in red. In contrast, the region containing metastases shows a low ECR value (70.0% ± 12.0%), as shown in yellowish-green and dark blue. Figure 2d and e are photomicrographs of normal lymph organization and regions containing metastases, respectively. The regions with metastases had lower cellular density than that ob-

Table 1
Cellular Density and ECR Values in Axillary Lymph Nodes*

	N	Cellular density ± SD (cells/μm^2)	MW-test	ECR (%)	MW-test
Normal lymph node	24	3.76 ± 0.67		130.7 ± 27.1	
			$P < 0.001$		$P < 0.001$
Metastasis lymph node	11	1.52 ± 0.67		60.6 ± 11.7	
			$P < 0.001$		$P < 0.001$
Adipose tissue	5	0.02 ± 0.01		2.1 ± 1.0	

*N is the number of axillary lymph nodes.

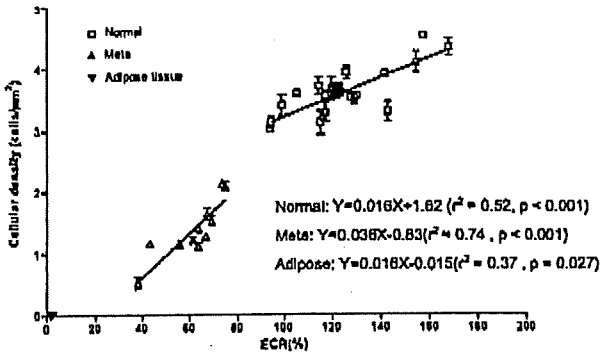

Figure 3. Correlation between cellular density and ECR value. The symbol □ is normal lymph node, △ is metastatic lymph node, and ▽ is adipose tissue.

served in regions of normal lymph organization. The WinRoof image shown in Fig. 2f was used to analyze cellular density for morphometry.

Table 1 lists the cellular densities and ECR values of axillary lymph nodes. Normal lymph nodes recorded the highest cellular density (3.76 ± 0.67 cells/μm^2) and the highest ECR values (130.7% ± 27.1%). Metastatic lymph nodes showed low cellular density (1.52 ± 0.67 cells/μm^2) and low ECR values (60.6% ± 11.7%). Adipose tissue had the lowest cellular density (0.02 ± 0.01 cells/μm^2) and the lowest ECR value (2.1% ± 1.0%). A statistically significant difference was obtained for both numerical values of each tissue ($P < 0.001$).

Figure 3 shows a correlation between cellular density and ECR value, in which the symbol □ represents normal lymph nodes, △ represents metastatic lymph nodes, and ▽ represents adipose tissue. Normal lymph nodes, metastatic lymph nodes, and adipose tissue formed separate clusters, with ECR values being related to cell density ($r^2 = 0.52$, $P < 0.001$; $r^2 = 0.74$, $P < 0.001$; and $r^2 = 0.37$, $P = 0.027$, respectively). Regression lines determined using cellular density as the outcome variable (y) and ECR values as the predictor variable (x) were $y = 0.016x + 1.62$ for normal lymph nodes, $y = 0.036x - 0.83$ for metastatic lymph nodes, and $y = 0.016x - 0.015$ for adipose tissue. The regression coefficient of the metastasis regression line was higher than that of normal lymph nodes.

Table 2 lists the sensitivity, specificity, efficiency, prevalence, positive predictive value, and negative predictive value of ECR in the ALND group. The ECR threshold used to judge the presence of metastasis is predicted to be 75% to 90%.

Evaluation of Axillary Lymph Nodes in the SLNB Group

Among the 35 patients in the SLNB group, 16 patients with a positive SLNB and two patients with a negative SLNB were selected to receive total ALND. The two negative patients were suspected to be false-negative cases in SLNB; ALND revealed inflammation in all lymph nodes. Of the 16 patients with a positive SLNB, seven patients had metastasis only in the SNL and nine patients had multiple metastatic lymph nodes. The threshold ECR value was evaluated for 35 lymph nodes from the results of the ALND group. Table 3 lists the sensitivity, specificity, efficiency, prevalence, positive predictive value, and negative predictive value of ECR in the SLNB group using a threshold ECR value of 80% for judging the presence of metastasis. The sensitivity, specificity, positive predictive value, and negative predictive value were 88.2%, 100%, 100%, and 92.6%, respectively, efficiency was 0.95, and prevalence was 0.40.

Among the 16 patients with a positive SLNB, two patients were micrometastasis and were false-negative by ECRI analysis. The images in Fig. 4 shows the axillary nodes of a patient with micrometastasis. Figure 4a is a 3DSPGR image. As seen in Fig. 4b and c, this lymph node seems free. However, this lymph node has micrometastases only to marginal sinus. In this lymph node, the ECR value and cellular density were 112.6% ± 15.4% and 4.86 ± 0.53 cells/μm^2, respectively. In another micrometastasis example, the ECR value and cellular density were 117.0% ± 16.4% and 4.59 ± 0.28 cells/μm^2, respectively. These measured values were equal to normal lymph node in Fig. 3.

DISCUSSION

Detection of metastasis in lymph nodes is important for optimum management of patients with cancer because it affects surgery, adjuvant chemotherapy and radiotherapy, and overall outlook. The majority of the previously reported MR studies that visualized the lymphatic system were performed with an intravenous injection of dextran-coated microparticles of iron oxide (9) or Ga-

Table 2
The Disorder Probability of ECR in the ALND Group

Threshold of ECR (%)	Sensitivity (%)	Specificity (%)	Efficiency	Prevalence	Positive predictive value (%)	Negative predictive value (%)
100	100	84	0.90	0.38	78.9	100
95	100	88	0.93	0.38	83.3	100
90	100	100	1.00	0.38	100	100
85	100	100	1.00	0.38	100	100
80	100	100	1.00	0.38	100	100
75	100	100	1.00	0.38	100	100
70	80	100	0.93	0.38	100	89.3
65	66.6	100	0.88	0.38	100	93.3
60	33.3	100	0.75	0.38	100	71.4

Table 3
The Disorder Probability of ECR in the SLNB Group*

Sensitivity (%)	88.2
Specificity (%)	100
Efficiency	0.95
Prevalence	0.40
Positive predictive value (%)	100
Negative predictive value (%)	92.6

*By employing an ECR value threshold of 80%.

domer-17, a conventional Gd-based contrast agent (10–12).

Cellular imaging is an important technique in developing treatment strategies and deciding the method of therapy, and its application in clinical medicine is at an early stage. The application of MRI to cellular imaging is expected to follow, as an in vivo examination. We demonstrated that ECRI is a feasible technique that does not require contrast injection for the detection of axillary lymph nodes in breast cancer (17,18). ECRI was able to quantitatively distinguish a change in the structural organization of the node; cellular components showed a high ECR value using the MRI parameters in this study (15,17,18). In the present study, with the aim of optimizing ALND and improving QOL, we performed axillary ECRI and evaluated both its utility as a cellular imaging technique and its accuracy as a predictor of axillary lymph node metastasis.

Color-mapped ECRI enables lymph node organization to be clearly visualized. Figure 1 shows images of an axillary lymph node without metastases; in contrast, Fig. 2 shows images of an axillary lymph node with metastases in which the regions of metastasis have lower cellular density and lower ECR values than that for normal lymph organization (Fig. 2e).

Figure 3 shows a correlation between cellular density and ECR value. Normal lymph nodes, metastatic lymph nodes, and adipose tissue formed separate clusters; the ECR values and cell densities are related for each cluster. Therefore, ECRI is a potentially useful method for cellular imaging of lymph nodes. The regression coefficient of the metastasis regression line was higher than that of normal lymph nodes; this shows that the cellular density of a lymph node changes greatly following metastasis. The ECR value fell with the presence of metastatic cells, epithelial tissue, and fibrous components (17,18); as a result, normal lymph nodes and metastatic lymph nodes formed two separate clusters. Because there is no repetition within the two clusters, the ECR value can definitively evaluate the presence or absence of lymph node metastasis by determining the threshold (Table 2).

In the SLNB group, we demonstrated the evaluation of axillary lymph node metastasis using the threshold ECR value (which judges the presence of metastasis) set at 80% (Table 3), which provides a most satisfactory result except a micrometastasis case. The ECR values obtained by our noninvasive method had sufficient sensitivity and specificity to detect axillary lymph node metastases. We consider that ECRI enables an individual lymph node to be evaluated as positive or negative for metastasis. In 16 patients with a positive SLNB, seven patients had only one metastatic lymph node. The results of ECRI were identical to the pathological findings; we suggest that these findings enable ALND to be confidently avoided.

It is thought that there is a limit in our method for detection of the micrometastasis case in which cellular density does not change. This study paid attention to a cellular component of a lymph node. ECRI of fibrous targets may be useful to evaluate marginal sinus (16). It was thought that collaboration with a molecular target chemical reagent was necessary in evaluation of the micrometastasis.

Adipose tissue had the lowest cellular density and ECR value (Table 1). We were easily able to recognize adipose tissue existing within a lymph node using ECRI. SLNB was negative, and two patients that caught ALND were equivalent to the case in Fig. 1. The ECR value of inflammatory tissue is high, like normal lymph node tissue. An inflammation can be distinguished from metastasis easily by removing adipose tissue from a measurement domain. The use of ECRI may help in eliminating inappropriate ALND.

Therefore, ECRI is potentially useful as a cellular density imaging technique in assessing the metastatic status of axillary lymph nodes in patients with breast carcinoma. In the SLNB, involvement of the axillary nodes with metastatic carcinoma can lead to mechanical obstruction of the lymphatic sinuses and alterations in fluid transport, which in turn may lead to a false-negative result if one was using a radiotracer or dye approach. It may be possible to reduce the number of false negatives in SLNB by excluding metastatic axillary lymph nodes using ECRI.

In conclusion, ECRI can provide insight into the adequacy of ALND and the prevention of complications

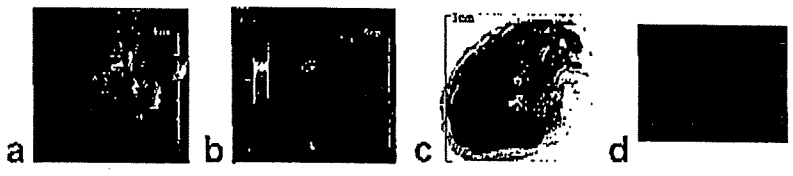

Figure 4. ECRI and photomicrograph of an axillary lymph node with micrometastases obtained from a patient with breast carcinoma. **a:** 3DSPGR image of the axillary lymph node. **b:** ECRI at frequency offset of 5 ppm. This lymph node shows a high ECR value (112.6% ± 15.4%), as shown in red on the ECRI. **c:** Macroscopic image of the lymph node (H&E stain; original magnification, ×5). The cellular density was 4.86 ± 0.53 cells/μm^2. **d:** High-power photomicrograph demonstrating normal lymph organization (H&E stain; original magnification, ×400). This lymph node has micrometastases only to marginal sinus.

such as lymphedema of the arm, thereby improving the QOL of patients with breast cancer.

ACKNOWLEDGMENTS

S.M. thanks Dr. Yasushi Yatabe at Aichi Cancer Center and Dr. Masaru Sogami at Gifu University Graduate School of Medicine for their valuable advice. S.M. also thanks Mr. Tetsuji Kurata and Mr. Mitsuhiro Uike at GE Yokogawa Systems, Ltd. for his kind support of this research.

REFERENCES

1. Sakorafas GH, Peros G, Cataliotti L, Vlastos G. Lymphedema following axillary lymph node dissection for breast cancer. Surg Oncol 2006;15:153–165.
2. Keshtgar MR, Ell PJ. Clinical role of sentinel-lymph-node biopsy in breast cancer. Lancet Oncol 2002;3:105–110.
3. Schuster DM, Halkar RK. Molecular imaging in breast cancer. Radiol Clin North Am 2004;42:885–908.
4. Moran PR, Hamilton CA. Near-resonance spin-lock contrast. Magn Reson Imaging 1995;13:837–846.
5. Era S, Sogami M, Kinosada Y, Matsushima S, Kato K, Nagai N. Magnetization transfer in protein solution gel, and polymer gel. In: Proceedings of the International Workshop on Magnetic Resonance and other Spectroscopic Techniques to Food Science. Harima, Japan, 1997. p 107–110.
6. Kobayashi H, Kawamoto S, Bernardo M, Brechbiel MW, Knopp MV, Choyke PL. Delivery of gadolinium-labeled nanoparticles to the sentinel lymph node: comparison of the sentinel node visualization and estimations of intra-nodal gadolinium concentration by the magnetic resonance imaging. J Control Release 2006;111:343–351.
7. Unno N, Inuzuka K, Suzuki M, et al. Preliminary experience with a novel fluorescence lymphography using indocyanine green in patients with secondary lymphedema. J Vasc Surg 2007;45:1016–1021.
8. Kobayashi H, Kawamoto S, Bernardo M, Brechbiel MW, Knopp MV, Choyke PL. Delivery of gadolinium-labeled nanoparticles to the sentinel lymph node: comparison of the sentinel node visualization and estimations of intra-nodal gadolinium concentration by the magnetic resonance imaging. J Control Release 2006;111:343–351.
9. Torchia MG, Nason R, Danzinger R, Lewis JM, Thliveris JA. Interstitial MR lymphangiography for the detection of sentinel lymph nodes. Surg Oncol 2001;78:151–156.
10. Torchia MG, Misselwitz B. Combined MR lymphangiography and MR imaging-guided needle localization of sentinel lymph nodes using Gadomer-17. AJR Am J Roentgenol 2002;179:1561–1565.
11. Suga K, Yuan Y, Ogasawara N, Okada M, Matsunaga N. Localization of breast sentinel lymph nodes by MR lymphography with a conventional gadolinium contrast agent. Preliminary observations in dogs and humans. Acta Radiol 2003;44:35–42.
12. Staatz G, Spuntrup E, Buecker A, Misselwitz B, Gunther RW. T1-weighted MR-lymphography after intramammary administration of Gadomer-17 in pigs. Rofo 2002;174:29–32.
13. Kobayashi H, Kawamoto S, Choyke PL, Sato N, Brechbiel MW. Comparison of dendrimer-based macromolecular contrast agents for dynamic micro-magnetic resonance lymphangiography. Magn Reson Med 2003;50:758–766.
14. Sogami M, Era S, Kinosada Y, et al. Basic studies on the equivalent cross-relaxation rate imaging (equivalent CRI) phantom studies. NMR Biomed 2001;367–375.
15. Matsushima S, Takasu A, Inai Y, et al. Equivalent cross-relaxation rate imaging in the synthetic copolymer gels and invasive ductal carcinoma of the breast. Magn Reson Imaging 2002;20:285–293.
16. Yuen S, Yamada K, Kinosada Y, et al. Equivalent cross-relaxation rate imaging of breast cancer. J Magn Reson Imaging 2004;20:56–65.
17. Matsushima S, Sasaki F, Sarumaru S, et al. Equivalent cross-relaxation rate image for decreasing a false negative case of sentinel node biopsy. Magn Reson Imaging 2003;21:1045–1047.
18. Matsushima S, Sasaki F, Yamaura H, et al. Equivalent cross-relaxation rate imaging for sentinel lymph node biopsy in breast carcinoma. Magn Reson Med 2005;54:1300–1304.
19. Zaremba L. FDA guidance for MR system safety and patient exposures: current status and future considerations. In: Magnetic resonance procedures: health effects and safety. Boca Ration, FL: CRC Press; 2001. p 183–196.

皮下埋め込み型中心静脈リザーバー（CVポート）の造設方法と合併症対策

稲葉吉隆*　山浦秀和**　佐藤洋造**　名嶋弥菜***
*愛知県がんセンター中央病院放射線診断IVR部・部長　**同・医長　***同・医局員

Keywords
皮下埋め込み型中心静脈リザーバー（CVポート）
インフューザー　ピンチオフエリア　カテーテル機能不全
血栓性静脈炎　薬剤の皮下漏出

皮下埋め込み型ポートと抗がん剤の投与

必要なときに体外から皮膚を介して穿刺し，体内に薬剤などを投与するための器具をポートまたはリザーバーとよび，目的部位内（血管内や腹腔内など）に挿入したカテーテルと接続して，皮下に埋め込み使用される．

ポートは埋め込み部位や体型により各種の形状があり，用途に応じて選択される．中心静脈ポート（CVポート）は，栄養点滴のみならず，抗がん剤の確実な静脈内投与経路として利用される頻度が大きくなっている．特に大腸がんに対する化学療法において，FOLFOX療法やFOLFIRI療法が標準療法として導入され，これらの療法には5-FUの持続静注が含まれ，これを外来ベースで運用するためには，中心静脈ポートと携帯用注入ポンプが必須であることが最大の理由である．

CVポートにおける器材の選択

ポートと接続して中心静脈内に留置されるカテーテルには，カテーテル先端がそのまま開口しているタイプ（通常のカテーテル）と，スリット状になり特殊弁となって開口するタイプ（グローションカテーテル〈先端盲端・側面スリット〉，オルカCVカテーテルキット〈先端スリット〉）があり，留置されているカテーテルがどのタイプなのか周知しておく必要がある．

1．先端開口型カテーテル

先端開口型では，通常の中心静脈カテーテルの場合と同様に薬液注入を終了し，抜針（抜管）時には血液の逆流による閉塞を防止するために，ヘパリン加生理的食塩水または生理的食塩水のみを充填する必要がある．

2．特殊弁型カテーテル

特殊弁型は，薬液注入時のみ開口し，血液逆流はしないようになっているので，あえてヘパリン加生理的食塩水を充填する必要はないとされている．

ポートそのものの選択は，大きさ，厚みが各種あるため，留置部位や皮下脂肪の状況などを考慮する．

CVポートの埋め込み位置の選択

通常の中心静脈カテーテルを挿入できる部位であれば，ポートの設置はおおむね可能である．ただし，安定したポートの設置に適した部位を考慮する必要がある．

1．カテーテル刺入血管の選択

カテーテル刺入血管は，腋窩～鎖骨下静脈が選択されることが多いが，内頸静脈，前腕静脈，上腕静脈，大腿静脈などからも可能で，施設間での差がみられる．

自己管理の面から，右利きの患者の場合は，左鎖骨下や左上肢にポートを設置することを推奨している施設もある．患者ごとに最適な部位で，解剖学的にポートの安定性がよく，患者の動きや生活に支障をきたさない部位が考慮されるべきである．

2．ピンチオフエリア

鎖骨下静脈を穿刺してカテーテルを留置する場合は，ピンチオフエリアとよばれる第1肋骨と鎖骨が交差する部位での穿刺は避け，それより外側の腋窩静脈領域での穿刺が推奨される．

カテーテルピンチオフとは，鎖骨下静脈に刺入されたカテーテルが第1肋骨と鎖骨に挟み込まれてカテーテルの閉塞や損傷をきたす現象で，鎖骨下静脈アプローチで挿入されたカテーテルに特有の合併症である．

当施設では，通常の中心静脈カテーテルの挿入と同様，右鎖骨下静脈（厳密には腋窩静脈内側部）よりカテーテルを挿入し，右鎖骨下前胸部にポートを設置することを第1選択としている．

CVポートの造設方法

1．造影透視や超音波を用いた静脈穿刺方法

カテーテルの挿入方法は，基本的には通常の中心静脈カテーテルの挿入法と同様であるが，従来の解剖学的指標をもとに穿刺する方法やX線透視下に穿刺する方法よりは，造影透視や超音波を用いて，穿刺する静脈を確認しながら穿刺する方法が推奨される．

2．ガイドワイヤーを用いるカテーテル挿入

静脈穿刺後はガイドワイヤーを用いて透視下操作により確実に目的部位までカテーテルを挿入する．皮下トンネルを通したカテーテルとポートを接続して，適切な位置に作成した皮下ポケットに埋設する．

以下に当施設での設置方法を紹介する．

①血管造影室，またはX線テレビ室にて行う．

②右肘静脈より造影剤を数mL注入し，右腋窩静脈から鎖骨下静脈の走行と開存性（まれではあるが，腕頭静脈で閉塞している症例が経験される）を透視下に確認し，おおよその穿刺位置や皮膚切開部位を決定する．

③消毒，局所麻酔後，ポートの大きさに合わせて皮膚切開し，皮下ポケットを作成する．

④再度，右肘静脈より造影剤を10～20mL注入し，右腋窩静脈から鎖骨下静脈の走行を透視下に確認しながら，皮切部より穿刺針を進めて静脈を穿刺する．第1肋骨の直上の腋窩静脈内側部を目標とする．

⑤静脈血の逆流を確認しガイドワイヤーを上大静脈まで進め，シース付きダイレーターを挿入する．

⑥当施設で使用している留置カテーテルは先端が特殊弁となっており，ガイドワイヤーに沿わせての挿入ができないためガイドワイヤーとダイレーターを抜去し，ピールアウェイシースからカテーテルを上大静脈まで挿入する．

⑦ピールアウェイシースを引き裂きながら抜去し，カテーテル先端位置を調節する．

⑧カテーテルの手元側は皮下ポケットの位置に合わせて切断しポートと接続し，ノンコアリング針でポートを穿刺して生理的食塩水でフラッシュして，カテーテル閉塞や損傷がないことを確認してから皮下に埋設する．

カテーテルの取り扱いや，カテーテルとポートの接続法は，個々の製品により異なるので，使用説明書により注意点を熟知しておく必要がある．

外来在宅化学療法の実際

外来担当医による当日の5-FU持続静注を含んだ化学療法（FOLFOX療法やFOLFIRI療法など）

実施可能の判断のもとに化学療法が開始される．

①ポート部皮膚面をアルコール綿で消毒し，生理的食塩水または注射用蒸留水入りのシリンジと接続したノンコアリング針（24G針を使用）でポートを穿刺する．

②ポート中央のセプタム部をポート底に当たるまでゆっくりと穿刺し，生理的食塩水または注射用蒸留水でポートからカテーテル内腔をフラッシュする．

③これによりポートシステムに異常がないことを確認し，薬液注入を開始する．ポートを穿刺する感覚，フラッシュする感覚を経験によりつかんでおくことが重要である．異常を感知した場合は，ポート設置医に連絡し確認する．

④5-FU持続静注はディスポーザブルの携帯用注入ポンプ（インフューザー）を用いて行う．規定用量の5-FUを生理的食塩水または注射用蒸留水により総量を調整して使用する．ディスポーザブルインフューザーは，温度，粘度，濃度により注入速度が異なってくるので，各製品の調整表に基づき総量を調整し，体温センサー（流量制御部）付きの製品は確実に皮膚面に貼り付ける．接続管の屈曲に注意して固定する．

カテーテル長期使用に伴うトラブルと対策

ポート設置部位により合併症にも差が生じることもあるが，共通注意事項を以下に述べる．

1）カテーテル機能不全（カテーテルピンチオフなどによるカテーテル損傷，フィブリンシースや，血栓，ねじれ，屈曲などによるカテーテル閉塞）

X線透視またはX線写真によりカテーテルの留置状況を確認し，必要に応じてポートからの造影を行い原因究明のうえ，原則としてシステムを抜去し再留置する．

血栓閉塞が疑われる場合は，生理的食塩水の圧入や血栓溶解剤の注入を試みることもあるが，強く圧入するとカテーテル損傷やカテーテル接続部離脱を招くことがあり，注意を要する．

2）血栓性静脈炎，静脈血栓症（カテーテル留置血管での血栓形成や静脈炎）

抗凝固療法，消炎剤や抗生物質の使用を検討する．症状によりシステムを抜去する．上大静脈症候群や肺動脈血栓・塞栓症を生じることもありうるので，十分な状態観察を要する．

3）薬剤の皮下漏出（穿刺針の抜漏，カテーテル損傷，カテーテル接続部離脱，ポートセプタム破損により発生）

システム損傷に起因する場合は抜去再留置する．穿刺針抜漏による場合は穿刺法やテープ固定法を再確認する．

抗がん剤の漏出時は早急にその処置（ステロイド局注など）を行い，状況により皮膚科専門医にコンサルトする．

4）皮膚障害（ポート被覆部皮膚発赤・びらん・潰瘍，ポート露出

発赤・びらん程度では一定期間不使用，軟膏処置で対応する．潰瘍形成やポート露出に至る場合や感染を伴う場合はシステム抜去を要する．皮膚形成が必要となる場合もある．

5）感染（カテーテル感染，ポート周囲感染）

カテーテル感染が疑われる場合（カテーテル吸引培養でも陰性のことも多い）は抗生物質の投与，カテーテル充填を試みるが，結局システム抜去が必要となることが多い．ポート周囲感染ではただちにシステムを抜去する．

いずれの場合も，ポート設置医（IVR医など）との連携を構築することが肝要である．

〈症例呈示〉

65歳男性．再発大腸がんに対して左腋窩静脈よりCVポートを設置し，FOLFOX療法施行中．

外来化学療法室において，左前胸部のポートを穿刺し，注射用蒸留水を注入したところ，通常より注入圧は低く，ポートの頭側皮下に疼痛が生じた．カテーテル損傷（注入圧抵抗の軽さからは断裂の可能性も）を想定し，胸部単純X線撮影を施

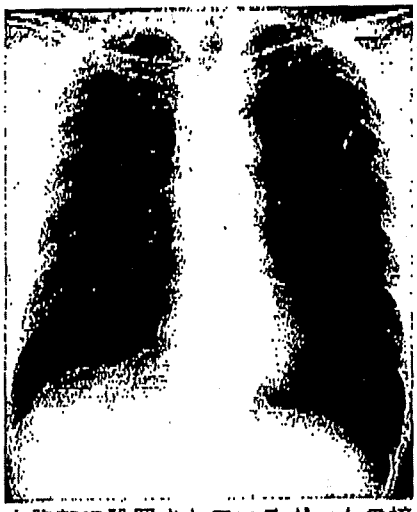

左胸部に設置されているポートの接続部に接続されているはずの留置カテーテルが認められない．この図では確認困難であるが，カテーテルは血管内に完全逸脱していた．

図1 カテーテル損傷を想定した胸部単純X線撮影

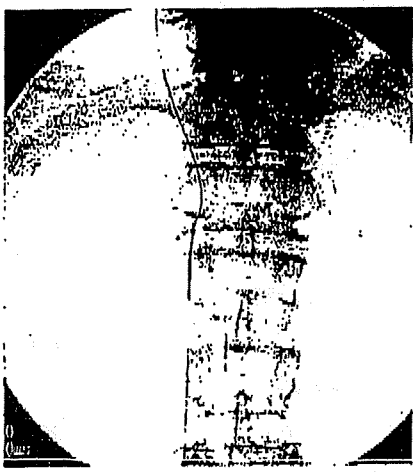

右大腿静脈より挿入したスネアカテーテルを用いて逸脱したカテーテルを把持し，回収した．

図2 スネアカテーテルを用いた断裂カテーテルの回収

行．カテーテルはポート接続部近傍で断裂しており，静脈内に完全逸脱していた（図1）．

放射線診断・IVR部にコンサルトがあり，患者に状況を説明後，右大腿静脈アプローチでスネアカテーテルを用いて断裂カテーテルを回収した（図2）．左前胸部を再切開し，カテーテルがはずれていたポートを抜去し，感染などのないことを確認し，CVポートを再設置した．

参考文献

1）Biffi R et al：A randomized, prospective trial of central venous ports connected to standard open-ended or Groshong catheters in adult oncology patients. Cancer, 92(5)：1204-1212, 2001.

2）Bjarnason H and Lehmann S：Central venous access, Castaneda-Zuniga WR ed, Interventional radiology, 3rd ed, Williams and Wilkins, 1997, p.941-965.

3）Hull JE, Hunter CS, and Luiken GA：The Groshong catheter：initial experience and early results of imaging-guided placement. Radiology, 185(3)：803-807, 1992.

4）坪井伸暁・他：前腕留置式埋没型中心静脈カテーテル法の長期成績，IVR会誌，18(4)：373-378, 2003.

5）Mansfield PF et al：Complications and failures of subclavian-vein catheterization. N Engl J Med, 331(26)：1735-1738, 1994.

6）黒岩俊郎・他：IVHポートの合併症について，IVR会誌，17(1)：39-43, 2002.

7）安井久晃・他：中心静脈カテーテル挿入・ポート造設の実際，管理，合併症とその対策．畠田安博・編，大腸がん標準化学療法の実際—FOLFOX/FOLFIRI療法の臨床導入，金原出版，2006, p.21-32.

8）Inaba Y et al：Central venous access port-related complications in outpatient chemotherapy for colorectal cancer. Jpn J Clin Oncol, 37(12)：951-954, 2007.